BNL-81288-2008-JA

MEASURING AEROSOL SIZE DISTRIBUTIONS WITH THE FAST INTEGRATED MOBILITY SPECTROMETER

Olfert, J. S., Kulkarni, P., and Wang, J.

Environmental Sciences Department/Atmospheric Sciences Division

Brookhaven National Laboratory
P.O. Box 5000
Upton, NY 11973-5000
www.bnl.gov

DISCLAIMER

Measuring aerosol size distributions with the fast integrated mobility spectrometer [⋆]

Jason S. Olfert [a], Pramod Kulkarni [b], Jian Wang [a,*]

[a] *Atmospheric Sciences Division, Brookhaven National Laboratory, Building 815E,*
Upton, NY 11973, USA

[b] *Centers for Disease Control and Prevention, National Institute for Occupational*
Safety and Health, 4676 Columbia Parkway, MS: R-5, Cincinnati, OH 45226,
USA

Abstract

A fast integrated mobility spectrometer (FIMS) has been developed for rapid aerosol size distribution measurements including those aerosols with low particle number concentrations. In this work, an inversion routine has been developed for the FIMS and it is demonstrated that the FIMS can accurately measure aerosol size distributions. The inversion routine includes corrections for the particle residence time in the FIMS and other factors related to the width of the response (or transfer) function and multiple charging of particles. Steady-state size distributions measured with the FIMS compared well with those measured by a scanning mobility particle sizer (SMPS). Experiments also show that the FIMS is able to capture the size distribution of rapidly changing aerosol populations. The total particle concentration integrated from distributions measured by the FIMS agrees well with simultaneous measurements by a condensation particle counter (CPC).

Key words: Aerosol size distribution, Fast response, Electrical mobility, Fast

1 Introduction

The measurement of sub-micrometer particle size distributions is important for a number of applications including the measurement of atmospheric aerosols and combustion-generated particles. In many of these applications, instruments with fast time responses are necessary to measure rapidly changing size distributions. In aircraft-based atmospheric aerosol studies, high time-resolution measurements are required to measure the size distributions of aerosols over small spatial domains. Furthermore, due to the relatively low particle concentrations in the atmosphere, an instrument built for such studies, must have good sensitivity, counting statistics, and size resolution.

Various instruments have been used to measure particle size distributions. The scanning mobility particle sizer (SMPS; Wang and Flagan, 1990), based on the differential mobility analyzer (DMA; Knutson and Whitby, 1975), is commonly used to determine size distributions and uses an electrical mobility technique. However, the minimum time required to measure a size distribution is on the order of 1 minute due to smearing effects in traditional CPCs. Faster SMPS measurements (as low as 3 s) are possible with fast-response mixing CPCs (Wang et al., 2002); however, with fast scan times, counting statistics deteriorate and there is increased uncertainty in the measurement. Much faster electrical mobility-based size distribution measurements (less than 1 s) are possible with the electrical aerosol spectrometer (EAS; Mirme et al., 1984) or with instruments derived from

---

* Corresponding author.

Email address: `jian@bnl.gov` (Jian Wang).

the EAS such as the differential mobility spectrometer (DMS; Reavell et al., 2002) and the engine exhaust particle sizer (EEPS; Johnson et al., 2004). These instruments charge the particles with a unipolar corona charger and the particles are detected by electrometer rings positioned lengthwise down a classification column. Although these instruments have fast response times, the sensitivity of the electrometers are relatively low, which limits these instruments to high concentration aerosol measurements such as engine exhaust measurements. Furthermore, due to the width of the unipolar charge distribution (and the uncertainty associated with it), the size resolution of these electrometer-based instruments is lower than that of the SMPS. The electrical low pressure impactor (ELPI, Keskinen et al. (1992)), measures aerodynamic size distributions with a time response < 5 s by charging particles with a unipolar charger and using electrometers mounted on the stages of a cascade impactor. However, the ELPI has poor size resolution for sub-micron particles and like EAS instruments, the sensitivity of the electrometers limits the ELPI to high aerosol concentrations. Aerosol size distributions can also be obtained by optical instruments such as optical particle counters (OPC), where the sizes of particles are derived from the intensity of light scattered by the particles. These instruments have good counting statistics and response times less than 1 s; however, they are generally limited to particles with diameters larger than 100 nm and there are often large uncertainties in the derived size distributions due to uncertainties in the particle morphology and refractive index (Hering and McMurry, 1991).

The above instruments have limited application in aircraft-based atmospheric studies or other applications where a fast time response and high sensitivity are required. Recently a new mobility-based particle-sizing instrument, called the fast integrated mobility spectrometer (FIMS), has been developed for such applications. In previous work, the concept and theory of the FIMS were presented (Kulkarni and Wang, 2006a) and a prototype was constructed and its performance was characterized in terms of sizing accuracy and

3

counting efficiency (Kulkarni and Wang, 2006b). The purpose of this paper is to describe an inversion routine that can be used to derive aerosol size distributions from the FIMS measurements. To determine the adequacy of the inversion routine, size distributions constructed from FIMS data were compared against size distributions measured with an SMPS. Furthermore, a transient aerosol was measured with the FIMS and a condensation particle counter (CPC) to demonstrate the fast response of the FIMS.

2 Operating principle of the FIMS

The operating principle and design of the FIMS is described in detail by Kulkarni and Wang (2006a,b). The FIMS consists of a charger, separator, condenser, and detector as shown in Figure 1. First, the aerosol passes through a bipolar radioactive charger, where the particles receive a bi-polar equilibrium charge distribution. The aerosol enters the separator, where a butanol-saturated sheath flow carries the particles in the y-direction. Inside the separator, under the influence of an electric field, charged particles are separated into different trajectories based on their electrical mobility (defined as the steady-state velocity of a charged particle divided by the strength of the electrostatic field). The classified particles are then carried by the sheath flow into the condenser, where no electric field is applied. Inside the condenser a supersaturation of butanol is generated through electrical cooling and the classified particles grow into super-micrometer droplets. At the exit of the condenser, a laser sheet illuminates the grown droplets, and their images are captured by a high-speed charge-coupled device (CCD) camera, which records particle images at 10 Hz. The images provide not only the particle concentration, but also the particle position, which is related to the particle electrical mobility, from which the particle size can be determined through data inversion.

The probability density function of the FIMS, $P(Z_{\mathrm{p}}, Z_{\mathrm{p}}^*)$, is the probability density of a

4

particle with an electrical mobility Z_p, when it enters the separator, will be classified at
the location defined by Z_p^*, where Z_p^* is called the instrument response electrical mobility.
The instrument response electrical mobility is defined as the centroid of the probability
density function for a particle with electrical mobility Z_p. It has been shown that the
instrument response electrical mobility of the FIMS is (Kulkarni and Wang, 2006a):

$$Z_\mathrm{p}^* = \frac{a}{bl_\mathrm{s}V}\left[Q_\mathrm{t}(3\tilde{x}^{*2} - 2\tilde{x}^{*3}) - Q_\mathrm{a}/2\right],\tag{1}$$

where a is the gap between the electrodes in the separator, b is the width of the sepa-
rator channel, l_s is the length of the separator, V is the voltage difference between the
electrodes, Q_a is the aerosol flow rate, Q_t is the total flow rate ($Q_\mathrm{t} = Q_\mathrm{sh} + Q_\mathrm{a}$, where Q_sh
is the sheath flow rate), and $\tilde{x}^*$ is the dimensionless distance from the ground electrode
where the particle has been detected ($\tilde{x}^* = x^*/a$).

3   Inversion of FIMS data

3.1   Method of data inversion

Inversion of the FIMS data is necessary to determine the size distribution of the particles
classified in the FIMS. The inversion routine uses the particle locations recorded on the
CCD image (the response of the instrument) to find the size distribution of the aerosol
that created such a response. Inversion is complicated by the fact that the same sized
particle can be counted at different locations due to the width of the probability density
function (defined above) and because of the multiple electrical charging of particles.

Inversion routines have been developed for previous particle sizing instruments and the
inversion of FIMS data is somewhat similar to the inversion procedures used in the DMA

5

(Hagen and Alofs, 1983) or SMPS (Collins et al., 2002). For a discrete set of measurements, R_i, the unknown size distribution can be found by solving a set of Fredholm integral equations:

$$R_i = \int\limits_{-\infty}^{\infty} K_i(d_\mathrm{p})n(\log d_\mathrm{p})\,\mathrm{d}\log d_\mathrm{p} + \varepsilon_i, \quad i = 1, 2, ..., I; \tag{2}$$

where R_i is the instrument response in channel i and I is the total number of channels. $K_i(d_\mathrm{p})$ is the response of channel i to a particle of diameter d_p and is often called the kernel function; it can be determined by theory or from calibration. $n(\log d_\mathrm{p})$ is the unknown particle number concentration with logarithms of diameter between $\log d_\mathrm{p}$ and $(\log d_\mathrm{p} + \mathrm{d}\log d_\mathrm{p})$. The particle number concentration is typically expressed in terms of $\log d_\mathrm{p}$ because aerosol size distributions are typically treated as lognormal and they cover several decades in particle size. The measurement uncertainty or instrument error in channel i is represented by ε_i.

The channels of an instrument vary from instrument to instrument. In a cascade impactor the channels are each stage of the impactor. In an SMPS system the channels are the discretized periods of time the DMA voltage is scanned. In the FIMS, images are recorded to determine the position of the classified particle. A schematic of an image is shown in Figure 2. In the FIMS, each image is divided into channels, which are equally spaced in terms of the logarithm of the particle diameter, between the minimum and maximum particle size that can accurately be determined (the following section describes how the channel limits are determined). The response of each channel, R_i, is simply the number of particles counted in the channel.

Since the data from the FIMS are discretized, the above integral can be approximated

6

with the rectangle rule and expressed as:

$$R_i \approx \sum_{j=1}^{J} K_i(d_{\mathrm{p}_j}) n(\log d_{\mathrm{p}_j}) \log\left(\frac{d_{\mathrm{p}_{j+1/2}}}{d_{\mathrm{p}_{j-1/2}}}\right) + \varepsilon_i, \tag{3}$$

where J is the number of 'size bins' (or size intervals over which the size distribution will be determined), d_{p_j} is the midpoint particle size of bin j, where $d_{\mathrm{p}_{j\pm1/2}}$ are the upper and lower bounds of the size bin, respectively; so that $d_{\mathrm{p}_j} = \sqrt{d_{\mathrm{p}_{j+1/2}} d_{\mathrm{p}_{j-1/2}}}$. Thus, we have a system of I equations with J unknowns. Equation 3 can be expressed in matrix form (neglecting the error terms) as:

$$\mathbf{R} = \mathbf{\Gamma} \mathbf{n}, \tag{4}$$

where $\mathbf{R}$ is an $I \times 1$ vector, $\mathbf{n}$ is an $J \times 1$ vector, and $\mathbf{\Gamma}$ is an $I \times J$ matrix, defined as $\Gamma_{ij} = K_{ij} \log\left(\frac{d_{\mathrm{p}_{j+1/2}}}{d_{\mathrm{p}_{j-1/2}}}\right)$.

The kernel of the FIMS, K_{ij}, is derived in detail in Appendix A and is given here:

$$K_{ij} = \frac{Q_a A_{\mathrm{view}} N_{\mathrm{F}}}{\dot{N}_{\mathrm{F}} ab} \bar{\eta}(d_{\mathrm{p}_j}) \left(\sum_{\phi=1}^{\phi_{\max}} \bar{f}(d_{\mathrm{p}_j}, \phi) \hat{\Omega}(Z_{\mathrm{p}}(d_{\mathrm{p}_j}, \phi), Z_{\mathrm{p}_i}^*, \sigma(d_{\mathrm{p}_j})) \right), \tag{5}$$

where $\dot{N}_{\mathrm{F}}$ is the frame rate of the camera, A_{view} is the area of the frame over which particle counting was performed, N_{F} is the total number of frames used to determine each size distribution, $\bar{\eta}(d_{\mathrm{p}_j})$ is a representative penetration efficiency for bin j, $\bar{f}(d_{\mathrm{p}_j}, \phi)$ is a representative charging probability for bin j, $\hat{\Omega}(Z_{\mathrm{p}}(d_{\mathrm{p}_j}, \phi), Z_{\mathrm{p}_i}^*, \sigma(d_{\mathrm{p}_j}))$ is the effective transfer function and it is the fraction of particles within bin j that are measured in channel i, and $\sigma(d_{\mathrm{p}_j})$ is the spread factor of the probability density function. These terms are described in more detail below.

The term $(Q_a A_{\mathrm{view}} N_{\mathrm{F}})/(\dot{N}_{\mathrm{F}} ab)$ is the total volume of aerosol used to determine one size distribution. Typically, the frame rate used in the FIMS is 10 Hz (although the current

7

camera can operate up to 60 Hz). If the aerosol is dilute, a size distribution constructed with 10 Hz data is often noisy due to the limited number of particle counts in each frame. Therefore, the size distributions are typically constructed using multiple frames, such as 10 frames for a 1 s-averaged size distribution. In this case, the instrument response, R_i, is the total particle counts in channel i in all N_{F} frames.

The particle penetration efficiency, $\bar{\eta}(d_{\mathrm{p}_j})$, is the product of the penetration efficiency of the tubing from the particle source to the FIMS inlet and the penetration efficiency of the FIMS inlet, which includes: 1) a Nafion dryer (MD-110-12S-4, Perma Pure LLC) to dry the aerosol, 2) an aerosol neutralizer (Model 3077A, TSI Inc.) to equalibriate the aerosol charge distribution, and 3) a laminar flow element to determine the aerosol flow rate. The penetration efficiency of the tubing from the particle source to the FIMS inlet was estimated from Hinds (1999). The particle penetration efficiency of the FIMS inlet was determined experimentally using a mono-disperse aerosol from a DMA and a condensation particle counter (CPC).

The charge probability, $\bar{f}(d_{\mathrm{p}_j}, \phi)$, is the probability that a particle of size d_{p} will have a certain number of elementary charges, ϕ. In this work, the charge probability was determined with the approximation for a bipolar charge distribution given by Wiedensohler (1988).

The effective transfer function, $\hat{\Omega}(Z_{\mathrm{p}}(d_{\mathrm{p}_j}, \phi), Z_{\mathrm{p}_i}^*, \sigma(d_{\mathrm{p}_j}))$, is defined as the fraction of particles with electrical mobilities between the limits $Z_{\mathrm{p}_{j-1/2}}$ and $Z_{\mathrm{p}_{j+1/2}}$ that are measured between the channel limits $Z_{\mathrm{p}_{i-1/2}}^*$ and $Z_{\mathrm{p}_{i+1/2}}^*$. The derivation of the effective transfer function is described in detail in Appendix A. Briefly, the transfer function is determined by integrating the probability density function, $P(Z_{\mathrm{p}_j}, Z_{\mathrm{p}_i}^*, \sigma)$, over each channel for the range of the particles from each size bin. The probability density function, as mentioned in Section 2, is the probability of a particle with an electrical mobility Z_{p}, when it enters

8

the separator, will be classified at the instrument response electrical mobility, Z_p^*. The probability density function of the FIMS was taken from Kulkarni and Wang (2006a), and takes into consideration the broadening of the probability density function due to particle diffusion. The spread factor $\sigma(d_{\mathrm{p}_j})$ determines the amount the probability density function widens due to particle diffusion (see Appendix A for details).

3.2 Instrument channel and size bin selection

In the FIMS, the response of the instrument, R_i, is determined by counting the particles in each channel from images taken with a high speed CCD camera. The channels are equally spaced in terms of the logarithm of the particle diameter. The width of each channel is determined by logarithmically spacing the size of each channel between the maximum and minimum particle diameter that can be accurately classified in the FIMS. It has been shown (Kulkarni and Wang, 2006a), that for a given operating condition, the theoretical maximum instrument response electrical mobility, (i.e. when $\tilde{x}^* = 1$ in Eq. 1) is $Z_{\mathrm{p}_{\max}}^* \approx \frac{aQ_\mathrm{sh}}{bl_\mathrm{s}V}$, while the minimum instrument response electrical mobility, (i.e. when $Q_\mathrm{t} = Q_\mathrm{a}$ in Eq. 1) is $Z_{\mathrm{p}_{\min}}^* = \frac{aQ_\mathrm{a}}{2bl_\mathrm{s}V}$. Practically, however, the range of electrical mobilities that can be accurately measured will be smaller than that mentioned. Particles cannot be counted very close to the wall due to uncertainties near the edges of the wall (such as butanol that has condensed on the wall), which result in missed or extra particle counts. Therefore, particle counts for $\tilde{x}^* > 0.95$ (or the region $\sim$0.6 mm closest the wall) were excluded and $Z_{\mathrm{p}_{\max}}^* = Z_\mathrm{p}^*(\tilde{x}^* = 0.95)$ from Eq. 1. Furthermore, the minimum instrument response electrical mobility for accurate measurements will be higher than the quantity stated above. In the FIMS, the width of the probability distribution function is relatively higher for smaller electrical mobilities, which means that the resolution of the instrument decreases for smaller electrical mobilities. Kulkarni and Wang (2006a) showed that for

9

adequate resolution the minimum instrument response electrical mobility should be 1/10 of the theoretical maximum (i.e. the range of the instrument is a factor of 10 in the electrical mobility). Therefore, we have used $Z^*_{\mathrm{p_{min}}} = 0.1\frac{aQ_{\mathrm{sh}}}{bl_{\mathrm{s}}V}$ in this work. From these electrical mobility limits, the upper and lower limits of the particle size channels, $d_{\mathrm{p_{max}}}$ and $d_{\mathrm{p_{min}}}$, are determined, where the electrical mobility is related to the diameter of a particle by:

$$Z_{\mathrm{p}} = \frac{\phi e C_{\mathrm{c}}(d_{\mathrm{p}})}{3\pi\mu d_{\mathrm{p}}}, \tag{6}$$

where e is the elementary unit of charge (1.60×10^{-19} C), and μ is the dynamic viscosity of the carrier gas. For a given geometry, the range of the instrument is dependant on the sheath flow rate and electrode voltage. For the operating conditions used in this work (see Table 1), the range of the instrument, in terms of the particle diameter was 32–122 nm. This size range may be too narrow for some applications. If a wider range is required, multiple FIMS units can be operated simultaneously, each measuring a different range in the size distribution. Kulkarni and Wang (2006a) showed that four FIMS units could cover a range of 5–1000 nm.

Once $d_{\mathrm{p_{max}}}$ and $d_{\mathrm{p_{min}}}$ have been determined, the channel limits ($d_{\mathrm{p}_{i-1/2}}$ and $d_{\mathrm{p}_{i+1/2}}$) can be calculated so that the limits are equally spaced in terms of $\log(d_{\mathrm{p}})$ between $d_{\mathrm{p_{max}}}$ and $d_{\mathrm{p_{min}}}$. The response of the FIMS for each image is then found by 1) calculating the electrical mobility of the channels limits ($Z^*_{\mathrm{p}_{i-1/2}}$ and $Z^*_{\mathrm{p}_{i+1/2}}$), 2) calculating the instrument response electrical mobility of each particle on the image (Z^*_{p}) from Eq.1, and 3) counting the particles within each channel.

The number of size bins, J, and their limits ($d_{\mathrm{p}_{j-1/2}}$ and $d_{\mathrm{p}_{j+1/2}}$) should be selected by considering the resolution of the instrument. To simplify the analysis, we have chosen to use the same number of channels as size bins ($I = J$) with the same spacing between

10

207 the channels and bins. Therefore, $d_{\mathrm{p}_{j-1/2}} = d_{\mathrm{p}_{i-1/2}}$ and $d_{\mathrm{p}_{j+1/2}} = d_{\mathrm{p}_{i+1/2}}$. The number of

208 channels and size bins that are used in this study was 10 ($I = J = 10$). The determination

209 of the number of channels is a trade off between size resolution and counting statistics.

210 With more channels the resolution of the determined size distribution increases but the

211 counting statistics in each bin decreases, increasing the uncertainty in each bin. Kulkarni

212 and Wang (2006a) showed that for a typical remote continental aerosol with a sampling

213 time of 1 s, good counting statistics are attained in the FIMS when 10 channels are

214 used. Therefore, 10 channels and size bins have been used in this work. One potential

215 advantage of the FIMS is that the number of channels and size bins can be adjusted in

216 post-processing. This is an important advantage in atmospheric studies since atmospheric

217 aerosols with fine structures in their size spectra are mostly observed near emission

218 sources and have high concentrations; therefore, an increased number of bins can be

219 used to capture the detailed structures. In contrast, away from emission sources, aerosols

220 typically have lower concentrations and less fine structures, so fewer channels/bins can

221 be used to improve counting statistics [1] .

222 *3.3 Time correction of FIMS data*

223 The velocity profile of the flow in the separator and condenser sections of the FIMS is non-

224 uniform. Particles of different electrical mobilities will travel with different trajectories in

225 the separator and condenser and, because of the parabolic profile of the carrier gas, they

226 will spend different times in each section. Therefore, at the end of the condenser, where

227 the image is recorded, the time each particle spent in the separator and condenser will

228 be different. To correct for this, the total residence time of each particle was calculated

---

[1] A similar technique can be used with the SMPS, but not with instruments such as the ELPI
or electrical aerosol spectrometers.

and the time the particle entered the separator was determined.

The particle residence time in the separator can be found by determining the position of the particle in the $\tilde{x}$-direction as a function of time. The motion of a particle in the $\tilde{x}$-direction in the separator is given by:

$$\frac{\mathrm{d}\tilde{x}}{\mathrm{d}t} = \frac{Z_\mathrm{p}E_x}{a} = \frac{Z_\mathrm{p}V}{a^2},\tag{7}$$

where, E_x is the electrostatic field strength. Assuming the gas flow is only in the y-direction, the time spent in the separator, t_s, can be found by integrating Eq. 7:

$$t_\mathrm{s} = \frac{\tilde{x}^* a^2}{Z_\mathrm{p}^* V},\tag{8}$$

where Z_p^* can be found using Eq. 1.

The velocity profile in the separator and condenser, $u_y(\tilde{x})$, is estimated as the velocity profile between two infinite parallel plates (i.e. we have neglected the effect of the edges of the channel), and is given by:

$$u_y(\tilde{x}) = \frac{6Q_\mathrm{t}}{ab}[\tilde{x}(1-\tilde{x})].\tag{9}$$

Since the location of the particles in the $\tilde{x}$-direction does not change in the condenser, the particle residence time in the condenser [2], t_c, is:

$$t_\mathrm{c} = \frac{l_\mathrm{c}ab}{6Q_\mathrm{t}[\tilde{x}^*(1-\tilde{x}^*)]},\tag{10}$$

---

[2] The velocity of particles in the x-direction is lost very quickly after the particles leave the electrostatic field since the relaxation time, and therefore the stopping distance, of the particles is so small. For example, a 50 nm particle classified in the FIMS has a stopping distance of 2.3×10^{-7} mm.

245 where l_c is the length of the classifier.

246 Therefore, the time from a particle entering the separator to being detected is $t_s + t_c$.
247 Figure 3 shows the travel times of particles in the separator and condenser as a function
248 of the final particle location, for operating conditions that we used in this work. The
249 figure shows that there is a time difference of several seconds between particles classified
250 near the center of the gap and those nearer the edge. Therefore, the time each particle
251 entered the separator was calculated, then the particles were sorted by time and binned
252 into new 'frames' with the same sampling rate as the camera frame rate.

253 *3.4 Other inversion considerations*

254 Further corrections should be made for accurate inversion of FIMS data. Firstly, particles
255 whose centroid electrical mobility diameter is outside the range of the FIMS may still be
256 classified by the FIMS because of the width of the probability density function. This will
257 result in an over-estimation of the particle concentration in the first and last size bins if
258 this is not corrected. This has the greatest effect on smaller electrical mobilities because
259 the probability density function is the widest at the smallest electrical mobility (Kulkarni
260 and Wang, 2006a)[3]. This error can be minimized by adding extra channels and bins at
261 each end of the response vector and the instrument kernel (as was done by Collins et al.
262 (2002)). Data is not available for the response vector, R, above the maximum instrument
263 response electrical mobility diameter so extrapolation is required. Instrument response
264 data is available for particles below the minimum instrument response electrical mobility
265 diameter. Recall that we set $Z^*_{p_{min}} = 0.1 \frac{aQ_{sh}}{bl_sV}$ and data were not used below this limit due

---

[3] It is interesting to note that the opposite is true for DMA data inversion, where the width
of the transfer function is higher for larger electrical mobilities due to the increased diffusivity
of the smaller particles.

13

to an increase in the uncertainty of this data. However, this data can be used to estimate particle concentrations below the lower limit, and this data can be directly incorporated into the inversion. In both cases, these extra size bins are added in the data inversion and then deleted after the inversion is complete.

Secondly, multiply-charged particles, whose singly-charged equivalent would have an electrical mobility less than the minimum instrument response electrical mobility diameter, will still be classified by the FIMS. This will result in extra particle counts in the upper channels (in terms of size) of the instrument. In general, the relative proportion of these particles will be small due to the nature of the charge distribution on the particles, so the error in the inverted size distribution will also be small. However, this error can be corrected by using an impactor at the inlet of the FIMS to remove particles larger than the maximum size of the FIMS measurement range, where it is assumed that the aerodynamic-equivalent diameter is approximately equal to the mobility-equivalent diameter of singly-charged particles (as is done with the impactors on TSI DMAs). However, this method may not be practical at very small particle sizes where the particle inertia is small. Another method for correcting the data is to use other instruments, such as an SMPS, OPC, or another FIMS unit operated at a larger size range, to determine the size distribution of aerosols larger than the size range of the instrument (as was done by Collins et al. (2002) for SMPS data). For transient measurements, the instrument measuring the larger size range should have the same, or better, time resolution than the FIMS, such as a OPC (which typically measure particles larger than 100 nm) or another FIMS operated at a larger size range.

If external size distributions are used to correct for this error, then the corrected instrument response, R_i', can be calculated with:

$$\mathbf{R}' = \mathbf{R} - \mathbf{\Gamma}_{\text{ext}}\mathbf{n}_{\text{ext}}, \tag{11}$$

14

where $\mathbf{\Gamma}_{\mathrm{ext}}$ is another kernel of the FIMS for particle sizes above the range of the FIMS, and $\mathbf{n}_{\mathrm{ext}}$ is the size distribution (in vector form) as determined by an external instrument. The kernel $K_{\mathrm{ext}_{ij}}$ is calculated using Eq. 5 for a new set of size bins. In this kernel, the size bins will range from the upper limit of the FIMS to the maximum particle size, which has ϕ_{max} charges, that will be classified in the FIMS measurement range. Five equally spaced size bins (in terms of logarithm) between these limits was used. More size bins only increases the computational time of the kernel calculation and has minimal effect on the correction. The size distribution $\mathbf{n}_{\mathrm{ext}}$ corresponds to the particle concentration measured by the external instrument at the logarithmic midpoint of each of the size bins. If for any reason a channel R'_i is less than zero (due to excessive under-counting in the FIMS, or excessive over-counting in the external instrument), then the channel is set to zero.

3.5 Solution of the inverse problem

From the above analysis the kernel matrix, $\mathbf{\Gamma}$, and the instrument response vector, $\mathbf{R}$, have been determined. Since we have chosen $I = J$, Eq. 4 can be solved exactly for the size distribution, $\mathbf{n}$, by: $\mathbf{n} = \mathbf{\Gamma}^{-1}\mathbf{R}$. However, because of noise in instrument measurements, this can lead to significant errors, oscillations, and negative values in the determined size distribution. An array of techniques have been developed to solve the inversion problem for aerosol size distributions including: linear methods (such as least-squared solutions and regularisation); non-linear iterative methods (such as Twomey's method); extreme value estimation; and Bayesian approaches. A good review of these methods is provided by Kandlikar and Ramachandran (1999). In this work, a slightly modified Twomey method has been used to invert the data because it is commonly used and it is simple to set up. The Twomey method has been described by Twomey (1975) and variations on the method

15

have been made by Markowski (1987) and Winklmayr et al. (1990). In the Twomey method an initial guess is iteratively multiplied by small multiples of the kernel function, which are proportional to the ratio of the actual instrument response to the calculated instrument response. The initial guess must be chosen so that it is positive to ensure that the final solution is positive. In this work, the initial guess was found solving, $\mathbf{n} = \mathbf{\Gamma}^{-1}\mathbf{R}$ exactly with Gaussian elimination. This initial guess may have negative values so any channels with values less than zero are set to zero. Then, similar to Markowski (1987) and Winklmayr et al. (1990), the initial guess is smoothed using a three term moving average:

$$
n_j = \begin{cases} \frac{3}{4}n_1 + \frac{1}{4}n_2, & j = 1, \\[2mm] \frac{1}{4}n_{j-1} + \frac{1}{2}n_j + \frac{1}{4}n_{j+1}, & \text{otherwise}, \\[2mm] \frac{1}{4}n_{J-1} + \frac{3}{4}n_J, & j = J. \end{cases} \tag{12}
$$

The smooth, positively-constrained initial guess was then input into the iterative Twomey routine. The Twomey routine was repeated until a chi-squared, χ^2, criteria was satisfied. The criteria was $\chi^2 < 1$ (i.e. the iterations were stopped when the calculated response was within the error range of the actual response) and iterations were also stopped if the change in χ^2 was less than 5% or if the newly calculated χ^2 was larger than the previous. Finally, the maximum number of iterations was limited to 100, because if none of the other criteria were matched with 100 iterations then it is unlikely that further iterations would improve the solution. In this work, χ^2 was defined as:

$$
\chi^2 = \frac{1}{I} \sum_{i=1}^{I} \left(\frac{(\mathbf{\Gamma}\mathbf{n}_{\text{new}})_i - R_i}{\varepsilon_i} \right)^2, \tag{13}
$$

where $\mathbf{n}_{\text{new}}$ is the latest size distribution from the last Twomey iteration and ε_i is the estimated absolute uncertainty in each channel. The absolute uncertainty of each channel

16

can be approximated, based on Poisson statistics, as $\varepsilon_i \approx \sqrt{R_i}$. Furthermore, the data from the extra bins mentioned in section 3.4 were not used in the χ^2 calculation.

4 Experimental setup

Experimental data are needed to demonstrate that the FIMS can accurately determine the size distributions of aerosols with the inversion routine discussed above. Aerosol size distributions were measured with the FIMS and with an SMPS and were compared. A condensation particle counter (CPC) was also used to compare the total number concentration of particles measured with the FIMS. A schematic of the experimental setup is shown in Figure 4. Sodium chloride (NaCl) particles were generated from a dilute solution of NaCl using an atomizer (Model 3076, TSI Inc.) and were dried with a silica gel diffusion drier. The particles passed through a filter by-pass dilution system, where the number concentration of the particles could be adjusted by increasing or decreasing the flow through a filter by controlling a valve on the by-pass line. The particles were passed through an aerosol neutralizer (Model 3077A, TSI Inc.) and were classified with a DMA (Model 3081, TSI Inc.). The DMA was used to produce an adjustable size distribution for comparing size distributions between the SMPS and the FIMS. The peak of the size distribution could be adjusted by changing the classifying voltage and the width of the distribution could be adjusted by changing the ratio of sheath to aerosol flow rate. The make-up air valve could be adjusted to control the aerosol flow rate in the DMA. In most of the experiments the ratio of sheath flow rate to aerosol flow rate was relatively low to produce a wide distribution (on the order of the range of the FIMS); where the sheath flow rate was set at 5.0 L/min and the aerosol flow rate was set at 3.9 L/min. An experiment was also conducted with a narrow (mono-disperse) distribution where the sheath and aerosol flow rates were 10 L/min and 1 L/min; respectively. The aerosol was typically

17

re-neutralized with an aerosol neutralizer and then measured with the FIMS, an SMPS (DMA column 3080L with CPC Model 3760A, TSI Inc.), and a CPC (Model 3076A, TSI Inc.). The aerosol was not re-neutralized in the experiment with the mono-disperse aerosol and the charging probability was adjusted accordingly in the kernel function (i.e. $\phi_{\max} = 1$ and $f(d_{\mathrm{p}}, \phi)$=1). As mentioned above, multiply-charged particles that are larger than the range of FIMS will still be classified by the FIMS and this should be corrected with an external size distribution. For the work shown here the external distribution was provided by the SMPS.

The FIMS was operated at the operating conditions shown in Table 1. Like the DMA, the ratio between the sheath flow and aerosol flow is an important variable determining the width of the transfer function. Kulkarni and Wang (2006a) showed that a ratio of sheath flow rate to aerosol flow rate of approximately 50 was a good compromise between size resolution and counting statistics; that ratio was used here. In order to avoid edge effects due to the ends of the channel, the area of view, A_{view}, used in the analysis was a 36 mm region spanning the center of the channel. Therefore, the area of view was: $a \times 36$ mm $= 4.02 \times 10^{-4}$ m^2. The measurement range of the FIMS can be adjusted by using different classifying voltages. For this study the classifying voltage was 700 V and with the operating conditions listed in Table 1, the measurement range of the FIMS, in terms of particle diameter, was approximately 32 – 122 nm.

The instrument response electrical mobility shown in Eq. 1 is an idealized case, which neglects the non-uniformity of the electric field at the entrance and exit of the separator, the edge effects of flow, and other non-uniform flow effects. The edge effects of the flow and weaker electrostatic forces at the exit of the separator will lead to lower than expected instrument response electrical mobilities. In Eq. 1 it is assumed that the flow rate in the FIMS is: $Q(\tilde{x}) = (Q_{\mathrm{sh}} + Q_{\mathrm{a}})(3\tilde{x}^2 - 2\tilde{x}^3)$, which assumes that the velocity profile is uniform in the z-direction (i.e. the flow is only parabolic in the x-direction). In reality, the flow will

18

be zero at the channel walls; consequently, the flow rate at the central area of view will be higher than the derived flow rate assuming no edge effects. An analytical series solution of laminar flow in a rectangular duct, given by Knudsen and Katz (1958), shows that the actual flow rate within the area, A_{view}, will be 5.6% higher than the flow rate assuming no edge effects. Therefore, the estimated instrument response electrical mobility will be lower than the actual value. To compensate for this discrepancy, effective flow rates (denoted with a *) can be used in the calculations, where $Q_t^* = 1.056(Q_{\text{sh}} + Q_{\text{a}}) = Q_{\text{sh}}^* + Q_{\text{a}}^*$. The edge effects on the aerosol flow rate, Q_{a}, will be very small due to the narrow aspect ratio of the aerosol inlet; therefore, we can assume that $Q_{\text{a}}^* \approx Q_{\text{a}}$. Thus the effective sheath flow rate will be, $Q_{\text{sh}}^* \approx 1.056Q_{\text{sh}} + 0.056Q_{\text{a}}$. Since the aerosol flow rate is typically 50 times smaller than the sheath flow rate this can be further simplified to: $Q_{\text{sh}}^* \approx 1.056Q_{\text{sh}}$. Furthermore, the FIMS was compared to a DMA to determine the effects of the other non-idealities on the actual instrument response electrical mobility. A DMA was used to produce a mono-disperse aerosol over a range of electrical mobilities ($Z_{\text{p,DMA}}$) and the expected instrument response electrical mobility, Z_{p}^*, was calculated using Eq. 1 (using the effective sheath flow rate mentioned above). Figure 5 shows a plot of the data, which have been fit with a line using least squares linear regression. The expected FIMS electrical mobility is very similar, yet consistently lower than the DMA electrical mobility, which is consistent with a weaker electrostatic field at the exit of the separator. The data are quite linear, so we can use an effective separator length to correct for the non-uniformities; where the effective length will be the actual length of the separator ($l_{\text{s}} = 112.1$ mm) multiplied by the slope of the fit line. Therefore, the effective length will be: $l_{\text{s}}^* = 0.987 \times 112.1$ mm $= 110.6$ mm. The effective sheath flow rate and effective length will be used in the calculations of the instrument response electrical mobility (Eq. 1), the channel/bin limits (see Sec. 3.2), the time correction (see Sec. 3.3), and the kernel (see App. A).

5 Experimental results and discussion

The ability of the FIMS to measure aerosol size distributions can be investigated by comparing size distributions measured with the FIMS with those measured by an SMPS. Three size distributions of NaCl particles and one ambient aerosol distribution were compared and are shown in Fig. 6(a)–(d). The figures show the average of approximately 10 minutes of data for the SMPS and FIMS. The scanning time of the SMPS was 2 minutes per distribution so the average of 5 distributions is shown. The FIMS recorded images at 10 Hz and size distributions were calculated for 2 minute intervals, therefore the FIMS distributions shown are also an average of 5 distributions. The error bars in the figures represent the standard deviation of the five distributions measured with each instrument. These error bars will be representative of the stability of the source aerosol and, too a lesser degree, the random variability in the inversion routines and the counting statistics. In the tests using NaCl particles (Figures 6(a)–(c)), the DMA was set to classification voltages corresponding to singly-charged particles of diameter 30, 60, and 100 nm (however, due to the broadness of the DMA transfer function used in these experiments, many larger multiply-charged particles would be classified as well).

In general, the agreement between the SMPS and the FIMS is good; the general shape and peak location of both distributions agree well. Table 2 summarizes the distribution parameters, such as total number concentration, N, geometric mean diameter, GMD, and geometric standard deviation, GSD, for both instruments [4]. The table shows that agreement between the FIMS and SMPS, in terms of GMD and GSD, is very good (within 3%). However, the number concentration of the FIMS measurements is higher

---

[4] These parameters must be compared over the same size range so the SMPS data was interpolated to the FIMS size bins and the distribution parameters were calculated using the interpolated size range.

than the SMPS measurements by 8–23% in these examples. The systematic difference in the number concentration between the FIMS and SMPS in this study may be due to uncertainties in the aerosol flow rates, the fluctuation of aerosol source, and also due to the uncertainties in the particle losses (or the correction for these losses) within the two instruments. Other measurements directly comparing the number concentration measured by the FIMS to the CPC 3760A (see Figure 8 and the discussion below) showed little to no systematic bias of the total number concentration. Furthermore, Kulkarni and Wang (2006b) showed good agreement between particle number concentrations measured by the FIMS and CPC 3760A over a range of particle sizes.

Figure 6(a) shows the comparison of a distribution with a peak of ∼30 nm. In this case the effect of multiple charging on the FIMS inversion routine is quite small, and the figure shows that the agreement is quite good, although the number concentration is higher than the peak of the SMPS distribution. In Figure 6(b) the peak of the distribution is ∼60 nm. In this case, the peak particle size of the FIMS distribution is slightly smaller compared to the SMPS peak size and the width of distributions are very similar. Figure 6(c) shows measured distributions with a peak of ∼100 nm. In this case the FIMS inversion is sensitive to multiply-charged particles whose singly-charged equivalent is larger than the range of the FIMS. As mentioned above, this was corrected with an external size distribution provided by the SMPS, and the figure shows that the distributions agree very well. The shoulder on the left-hand side of the distribution is resolved by both the FIMS and the SMPS. The figure also shows the calculated FIMS distribution without using the external correction from the SMPS data. This distribution is very similar to the standard FIMS distribution at smaller particle sizes, but at larger particle sizes the number concentration is higher as would be expected. The Figure 6(d) compares measurements of an ambient aerosol (the aerosol was not pre-classified with the DMA) and again the agreement between the instruments is good.

21

The FIMS and SMPS were also used to measure the size distribution of a 'mono-disperse' aerosol from a DMA, and the results are plotted in Figure 7. The figure shows measurements made with the FIMS and the SMPS, as well as the expected distribution from the DMA. The expected DMA distribution was calculated using the the width of the non-diffusive transfer function determined by Knutson and Whitby (1975) for the DMA operating conditions and the height was the height that gave the same total number concentration as that measured by the SMPS. The actual transfer function of the DMA will be slightly wider due to particle diffusion, but that is neglected here. Two inversions are shown of the FIMS data. The first inversion is the standard inversion with 10 channels/bins and with the smoothing function shown in Eq. 12, the second inversion uses 30 channels/bins and without the smoothing function. The figure shows that size distributions measured with the FIMS with the standard inversion is considerably wider than the actual size distribution. This is expected due to the limited number of channels used in this inversion and also due to data smoothing. As discussed in section 3.2, more channels/bins can be used for better size resolution if particle concentrations are adequate for acceptable counting statistics. This is shown here where the FIMS inversion with 30 channels/bins and without data smoothing represents the actual size distribution much better and is very similar to the SMPS measurement, although both measurements are slightly wider than the expected mono-disperse distribution. The peak particle size of the FIMS and SMPS distributions are both slightly lower than the expected DMA particle size, which may be due to uncertainties in the DMA operating conditions (i.e. sheath flow rate or classifying voltage) or due to the non-uniformity of the initial particle distribution from which the mono-disperse particles were classified.

An important aspect of the FIMS is its ability to measure size distributions with a fast time response. A rapidly changing size distribution was used to demonstrate the rapid response of the FIMS. The dilution system was used to create a transient size distribution

22

by rapidly adjusting the dilution ratio and 1 s-averaged size distributions measured by the FIMS are shown in Figure 8(a). The total particle number concentration can be determined with the FIMS by integrating the size distribution. A time series plot of the total number of concentration measured by a CPC 3760A and the FIMS is shown in Figure 8(b). Firstly, the figure shows that the measurements of the total number concentration derived from the FIMS size distribution agrees very well with the CPC. Presumably the higher noise levels in the FIMS data (the CPC data is also averaged over 1 second) is due to the lower sampling flow rate and counting statics in the FIMS. Secondly, the close agreement between the FIMS and CPC suggest that the FIMS is capable of accurately characterizing rapid variations in size distributions, even for aerosol with low particle concentrations.

6   Summary

The fast integrated mobility spectrometer (FIMS) was developed in order to make rapid measurements of aerosol size distributions. The FIMS simultaneously measures particles of different sizes through single particle detection, and is capable of rapid measurements with excellent counting statistics, even for aerosols with low particle concentrations. In previous work, the concept, the theory, and a prototype of a FIMS were presented (Kulkarni and Wang, 2006a,b). In the present work, an inversion routine was developed to derive aerosol size distributions from FIMS measurements. The FIMS data was inverted by numerically solving a set of Fredholm integral equations using the Twomey method, which is an iterative routine that corrects an initial guess until the solution agrees (within error limits) with the instrument response. The inversion routine for the FIMS included a time correction for the particle data because particles with different electrical mobilities will have different residence times in the FIMS. The inversion routine also took into consid-

23

eration the width of the probability density function near the limits of the FIMS range as well as for large multiply-charged particles whose singly-charged equivalent would be outside the mobility range of the FIMS. The inversion routine was used to determine aerosol size distributions, which were compared to simultaneous SMPS measurements. In general, the agreement between the instruments was very good for a wide range of aerosol spectra, including cases in which multiple-charged particle outside of the FIMS measurement range contribute substantially to the number of particles detected. The rapid response of the FIMS was demonstrated by measuring a transient aerosol. The FIMS was able to capture the rapid variation in aerosol size distribution, and the total particle concentration integrated from the size distribution agreed closely with direct measurements by a CPC.

Acknowledgements

24

A The kernel of the FIMS

This appendix describes the method used to determine the kernel of the FIMS, K, used in the inversion calculations. The kernel is defined as the fraction of particles from size bin j that is measured in channel i, Ψ_{ij}, multiplied by the total volume of aerosol measured in each size distribution, V_{a}. Therefore;

$$K_{ij} \equiv V_{\mathrm{a}} \Psi_{ij}. \tag{A.1}$$

The volume of aerosol measured in each size distribution, V_{a}, is the aerosol volumetric flow rate, Q_{a}, multiplied by the length of time each size distribution is measured, t_{a}. In the FIMS, the high speed CCD camera captures images with a frame rate, $\dot{N}_{\mathrm{F}}$. Therefore, t_{a} will equal the total number of frames used to construct each size distribution, N_{F}, divided by the camera frame rate. Furthermore, the entire width of the classification channel (b) is not used (in order to avoid edge effects), so V_{a} must be corrected by the ratio of the area of the channel used, A_{view}, divided by the total area of the classification channel, ab. Therefore, the volume of aerosol measured in each size distribution is:

$$V_{\mathrm{a}} = Q_{\mathrm{a}} t_{\mathrm{a}} \frac{A_{\mathrm{view}}}{ab} = Q_{\mathrm{a}} \frac{N_{\mathrm{F}}}{\dot{N}_{\mathrm{F}}} \frac{A_{\mathrm{view}}}{ab}. \tag{A.2}$$

The fraction of particles from size bin j that is measured in channel i, Ψ_{ij}, is determined by theory and must consider particle charging and particle losses. Kulkarni and Wang (2006a) have determined a probability density function (that includes the effects of particle diffusion), which is the probability density that a particle with electrical mobility Z_{p} will be measured at the normalized instrument electrical mobility $\tilde{Z}_{\mathrm{p}}^{*}$, where $\tilde{Z}_{\mathrm{p}}^{*} = Z_{\mathrm{p}}^{*}/Z_{\mathrm{p}}$. The probability density function, $P(Z_{\mathrm{p}}, \tilde{Z}_{\mathrm{p}}^{*})$, is (Kulkarni and Wang, 2006a, Eq. 43):

$$P(Z_{\mathrm{p}}, \tilde{Z}_{\mathrm{p}}^{*}, \sigma) = \frac{1}{2\Delta \tilde{Z}_{\mathrm{p}}^{*}} \left[\mathrm{erf}\left(\frac{\tilde{Z}_{\mathrm{p}}^{*} - 1 + \frac{1}{2}\Delta \tilde{Z}_{\mathrm{p}}^{*}}{\sigma} \right) - \mathrm{erf}\left(\frac{\tilde{Z}_{\mathrm{p}}^{*} - 1 - \frac{1}{2}\Delta \tilde{Z}_{\mathrm{p}}^{*}}{\sigma} \right) \right], \tag{A.3}$$

25

where $\Delta \tilde{Z}_{\mathrm{p}}^* = \Delta Z_{\mathrm{p}}^*/Z_{\mathrm{p}} = (\frac{Q_{\mathrm{a}}a}{bl_{\mathrm{s}}V})/Z_{\mathrm{p}}$ and σ is the dimensionless spread factor that charac-

terizes the broadening of the probability density function due to particle diffusion. The

spread factor is given by Kulkarni and Wang (2006a):

$$\sigma(d_{\mathrm{p}})^2 = \frac{1}{\mathrm{Pe}}\left[2\tilde{x}^*\left(\frac{a}{l_{\mathrm{s}}}\right)^2 + 72\left(1 + \frac{Q_{\mathrm{a}}}{Q_{\mathrm{sh}}}\right)^2\left(\frac{\Delta\tilde{Z}_{\mathrm{p}}^*}{Q_{\mathrm{a}}/Q_{\mathrm{sh}}}\right)^2\left(\frac{\tilde{x}^{*3}}{3} - \frac{\tilde{x}^{*4}}{2} + \frac{\tilde{x}^{*5}}{5}\right)\right], \quad \text{(A.4)}$$

where Pe is the Peclet number and $\tilde{x}^*$ is the dimensionless location of the centroid particle

trajectory at the exit of the separator. The Peclet number is a dimensionless number

relating the rate of advection of a particle to its rate of diffusion; $\mathrm{Pe} = Z_{\mathrm{p}}V/D$, where D

is the particle diffusivity. $\tilde{x}^*$ can be found by solving Eq. 1 using a numerical root-finding

technique.

The probability, Ω, that a particle with electrical mobility Z_{p} will be classified between

the instrument response electrical mobilities $\tilde{Z}_{\mathrm{p}}^*$ and $\mathrm{d}\tilde{Z}_{\mathrm{p}}^*$ is:

$$\Omega = \int P(Z_{\mathrm{p}}, \tilde{Z}_{\mathrm{p}}^*, \sigma)\,\mathrm{d}\tilde{Z}_{\mathrm{p}}^*. \quad \text{(A.5)}$$

For the kernel calculation, we wish to determine the fraction of particles within size bin

j that is measured in channel i, Ψ_{ij}. This will be the fraction of particles with electrical

mobilities between the limits $Z_{\mathrm{p}_{j-1/2}}$ and $Z_{\mathrm{p}_{j+1/2}}$ that are measured between the channel

limits $\tilde{Z}_{\mathrm{p}_{i-1/2}}^*$ and $\tilde{Z}_{\mathrm{p}_{i+1/2}}^*$ (this will be called the effective transfer function, $\hat{\Omega}$), multiplied

by the charge probability of each particle for each number of elementary charges, ϕ,

multiplied by the particle penetration efficiency of the FIMS inlet, $\eta(d_{\mathrm{p}_j})$. Therefore,

26

using the probability density function described above, Ψ will be:

$$\Psi_{ij} = \frac{\displaystyle\sum_{\phi=1}^{\phi_{\max}} \int_{Z_{\mathrm{P}_{j-1/2}}}^{Z_{\mathrm{P}_{j+1/2}}} \int_{\tilde{Z}^*_{\mathrm{P}_{i-1/2}}}^{\tilde{Z}^*_{\mathrm{P}_{i+1/2}}} \eta(d_{\mathrm{p}_j}) f(d_{\mathrm{p}_j}, \phi) P(Z_{\mathrm{p}_j}, \tilde{Z}^*_{\mathrm{p}_i}, \sigma)\, \mathrm{d}\tilde{Z}^*_{\mathrm{p}_i}\, \mathrm{d}Z_{\mathrm{p}_j}}{\displaystyle\int_{Z_{\mathrm{P}_{j-1/2}}}^{Z_{\mathrm{P}_{j+1/2}}} \mathrm{d}Z_{\mathrm{p}_j}}. \tag{A.6}$$

We may assume that the charge probability, $f(d_{\mathrm{p}_j}, \phi)$, and the particle penetration efficiency, $\eta(d_{\mathrm{p}_j})$, are constant for each bin j since the change in each term over the width of one size bin is relatively small. This assumption greatly reduces the number of calculations needed to calculate the kernel numerically and has little effect on the solution. Therefore, we can use a representative charge probability, $\bar{f}(d_{\mathrm{p}_j}, \phi)$, and penetration efficiency, $\bar{\eta}(d_{\mathrm{p}_j})$, which in this work was the charge probability and penetration efficiency at the center of each size bin. Therefore, Eq. A.6 simplifies to:

$$\Psi_{ij} = \bar{\eta}(d_{\mathrm{p}_j}) \sum_{\phi=1}^{\phi_{\max}} \bar{f}(d_{\mathrm{p}_j}, \phi) \frac{\displaystyle\int_{Z_{\mathrm{P}_{j-1/2}}}^{Z_{\mathrm{P}_{j+1/2}}} \int_{\tilde{Z}^*_{\mathrm{P}_{i-1/2}}}^{\tilde{Z}^*_{\mathrm{P}_{i+1/2}}} P(Z_{\mathrm{p}_j}, \tilde{Z}^*_{\mathrm{p}_i}, \sigma)\, \mathrm{d}\tilde{Z}^*_{\mathrm{p}_i}\, \mathrm{d}Z_{\mathrm{p}_j}}{Z_{\mathrm{P}_{j+1/2}} - Z_{\mathrm{P}_{j-1/2}}} \tag{A.7}$$

$$= \bar{\eta}(d_{\mathrm{p}_j}) \sum_{\phi=1}^{\phi_{\max}} \bar{f}(d_{\mathrm{p}_j}, \phi) \hat{\Omega}(Z_{\mathrm{p}_j}(d_{\mathrm{p}_j}, \phi), Z^*_{\mathrm{p}_i}, \sigma(d_{\mathrm{p}_j})). \tag{A.8}$$

The double integral can be determined numerically using the trapezoidal rule. For this work, we have used 50 steps in each bin j and channel i; increasing the number of steps had little effect on the calculated transfer function and only increased the computational time.

Therefore, the kernel of the FIMS is:

$$K_{ij} = Q_{\mathrm{a}} \frac{N_{\mathrm{F}}}{\dot{N}_{\mathrm{F}}} \frac{A_{\mathrm{view}}}{ab} \bar{\eta}(d_{\mathrm{p}_j}) \sum_{\phi=1}^{\phi_{\max}} \bar{f}(d_{\mathrm{p}_j}, \phi) \hat{\Omega}(Z_{\mathrm{p}_j}(d_{\mathrm{p}_j}, \phi), Z^*_{\mathrm{p}_i}, \sigma(d_{\mathrm{p}_j})). \tag{A.9}$$

27

References

Collins, D. R., Flagan, R. C., Seinfeld, J. H. (2002). Improved inversion of scanning DMA data. *Aerosol Science and Technology, 36*, 1–9.

Hagen, D. E., Alofs, D. J. (1983). Linear inversion method to obtain aerosol size distributions from measurements with a differential mobility analyzer. *Aerosol Science and Technology, 2*, 465–475.

Hering, S. V., McMurry, P. H. (1991). Optical counter response to monodisperse atmospheric aerosols. *Atmospheric Environment, 25A*, 463–468.

Hinds, W. C. (1999). *Aerosol Technology — Properties, Behavior, and Measurement of Airborne Particles.* John Wiley and Sons.

Johnson, T., Caldow, R., Pocher, A., Mirme, A., Kittelson, D. B. (2004). An engine exhaust particle sizer spectrometer for transient emission particle measurements. *Society of Automotive Engineers.* 2004-01-1341.

Kandlikar, M., Ramachandran, G. (1999). Inverse methods for analysing aerosol spectrometer measurements: A critical review. *Journal of Aerosol Science, 30*, 413–437.

Keskinen, J., Pietarinen, K., Lehtimäki, M. (1992). Electrical low pressure impactor. *Journal of Aerosol Science, 23*, 353–360.

Knudsen, J. G., Katz, D. L. (1958). *Fluid dynamics and heat transfer.* McGraw-Hill.

Knutson, E. O., Whitby, K. T. (1975). Aerosol classification by electric mobility: Apparatus, theory, and applications. *Journal of Aerosol Science, 6*, 443–451.

Kulkarni, P., Wang, J. (2006a). New fast integrated mobility spectrometer for real-time measurement of aerosol size distribution – I: Concept and theory. *Journal of Aerosol Science, 37*, 1303–1325.

Kulkarni, P., Wang, J. (2006b). New fast integrated mobility spectrometer for real-time measurement of aerosol size distribution: II. Design, calibration, and performance characterization. *Journal of Aerosol Science, 37*, 1326–1339.

28

Markowski, G. R. (1987). Improving Twomey's algorithm for inversion of aerosol measurement data. *Aerosol Science and Technology, 7*, 127–141.

Mirme, A., Noppel, M., Piel, I., Salm, J., Tamm, E., Tammet, H. (1984). Multi-channel electric aerosol spectrometer. *11th international conference on atmospheric aerosols, condensation and ice nuclei.* Vol. 2, Budapest, pp. 155–159.

Reavell, K., Hands, T., Collings, N. (2002). A fast response particulate spectrometer for combustion aerosols. *Society of Automotive Engineers.* 2002-01-2714.

Twomey, S. (1975). Comparison of constrained linear inversion and an iterative nonlinear algorithm applied to the indirect estimation of particle size distributions. *Journal of Computational Physics, 18*, 188–200.

Wang, J., McNeill, V. F., Collins, D. R., Flagan, R. C. (2002). Fast mixing condensation nucleus counter: Application to rapid scanning differential mobility analyzer measurements. *Aerosol Science and Technology, 36*, 678–689.

Wang, S. C., Flagan, R. C. (1990). Scanning electrical mobility spectrometer. *Aerosol Science and Technology, 13*, 230–240.

Wiedensohler, A. (1988). An approximation of the bipolar charge distribution for particles in the submicron size range. *Journal of Aerosol Science, 19*, 387–389.

Winklmayr, W., Wang, H.-C., John, W. (1990). Adaptation of the Twomey algorithm to the inversion of cascade impactor data. *Aerosol Science and Technology, 13*, 322–331.
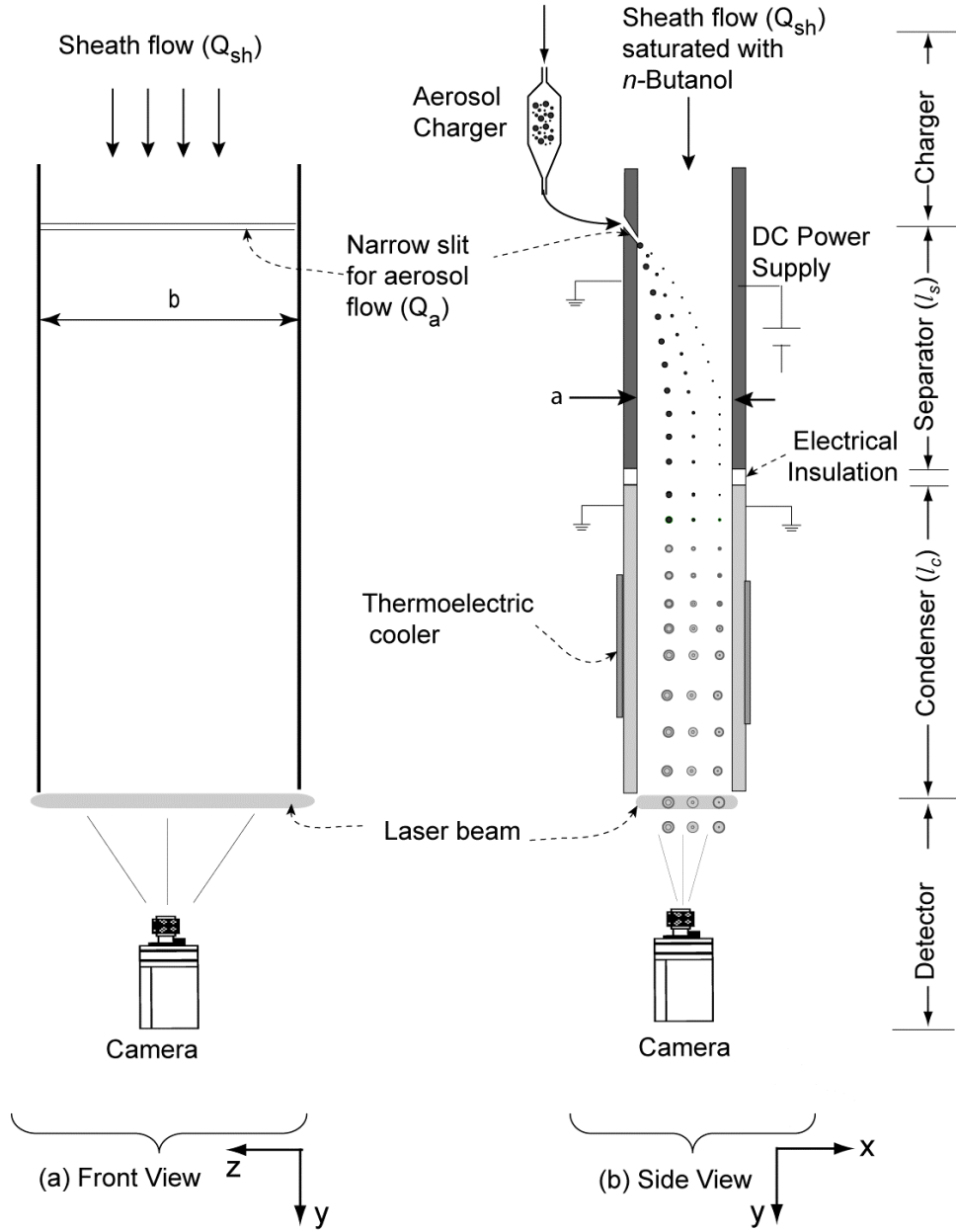
29

Figure Captions

- Figure 1: Schematic of the fast integrated mobility spectrometer.

- Figure 2: Schematic of an image from the FIMS (not to scale). Each image is divided into I channels, the channels are equally spaced in terms of $\log(d_{\mathrm{p}})$, where $d_{\mathrm{p}_{i-1/2}}$ and $d_{\mathrm{p}_{i+1/2}}$ represent the lower and upper bounds of channel i. The response of each channel, R_i, is the number of particles counted in the channel.

- Figure 3: The time each particle spends in the separator (t_{s}), the condenser (t_{c}), and the total ($t_{\mathrm{s}} + t_{\mathrm{c}}$) as a function of the particle location, $\tilde{x}^* = x^*/a$, for the operating conditions shown in Table 1.

- Figure 4: Schematic of the experimental setup.

- Figure 5: Calibration curve for the FIMS, where $Z_{\mathrm{p,DMA}}$ is the electrical mobility of particles from the DMA and Z_{p}^* is the expected instrument response electrical mobility of the FIMS (see Eq. 1).

- Figure 6: Comparisons of aerosol size distributions measured with the FIMS and SMPS. Figures (a)–(c) are comparisons of DMA-classified NaCl particles. Figure (d) is a comparison of an ambient aerosol.

- Figure 7: Comparison of a 60 nm mono-disperse aerosol measured with the FIMS and SMPS. The FIMS inversion was carried out with the standard inversion (10 channels with smoothing, shown as '△') and with an inversion with 30 channels and without the smoothing function shown in Equation 12 (shown as '◇'). The expected distribution from the DMA (calculated from the operating conditions of the DMA) is also shown.

- Figure 8: Measurements of a transient aerosol: (a) size distribution measured with the FIMS, (b) total number concentration of the same aerosol measured with the FIMS and CPC.

Table 1

Dimensions and operating conditions of the FIMS

Dimension or Operating Condition	Value
Distance between electrodes, a	11.18 mm
Width of channel, b	127.0 mm
Effective length of separator, l_s^*	110.6 mm
Length of condenser, l_c	319.3 mm
Effective sheath flow rate, Q_{sh}^*	12.7 L/min
Aerosol flow rate, Q_a	0.24 L/min
Voltage, V	700 V
Camera frame rate, $\dot{N}_F$	10.0 Hz
Area of view in image, A_{view}	$(a \times 36 \text{ mm}) = 4.02 \times 10^{-4} \text{ m}^2$

Table 2. Comparison of the FIMS and SMPS size distribution parameters

	Fig. 6(a)			Fig. 6(b)			Fig. 6(c)			Fig. 6(d)		
	FIMS	SMPS	% diff.	FIMS	SMPS	% diff.	FIMS	SMPS	% diff.	FIMS	SMPS	% diff.
N (cm^{-3}) [a]	920	707	23%	638	509	20%	619	509	18%	5990	5540	8%
GMD (nm) [b]	39.6	39.9	-1%	61.1	63.0	-3%	81.6	83.1	-2%	46.7	46.1	1%
GSD [c]	1.19	1.20	-1%	1.34	1.32	2%	1.31	1.28	2%	1.39	1.39	1%

[a] Total particle number concentration

[b] Geometric mean diameter

[c] Geometric standard deviation

Fig. 1. Schematic of the fast integrated mobility spectrometer.
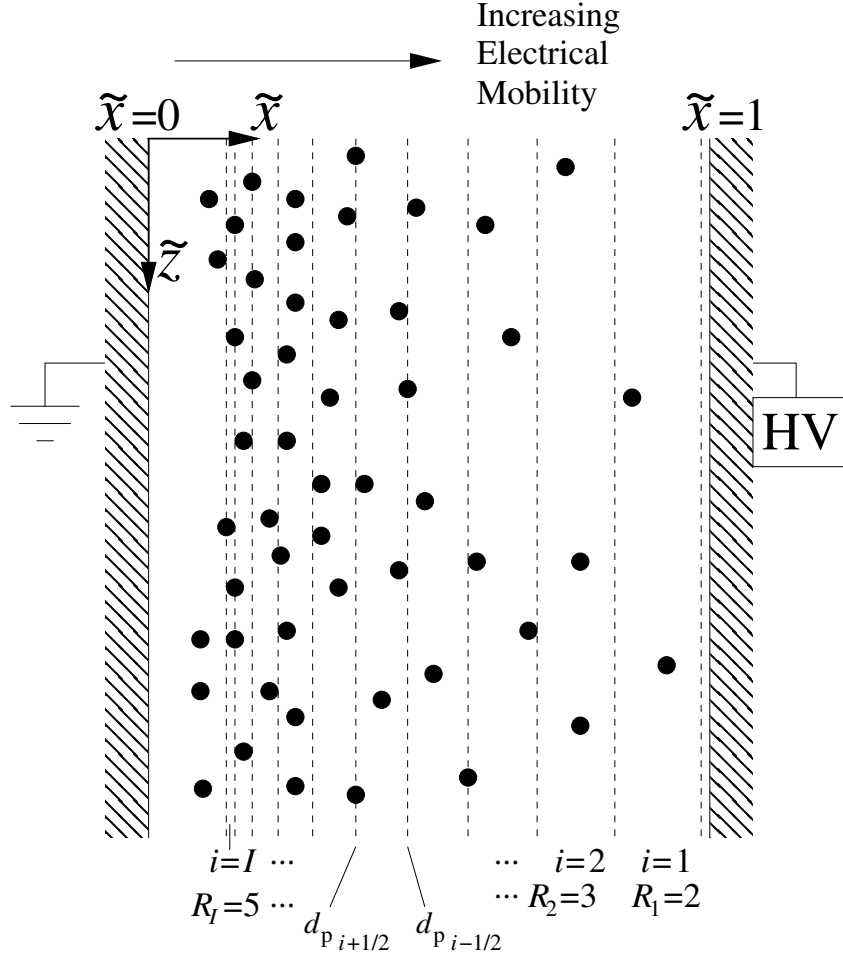
Fig. 2. Schematic of an image from the FIMS (not to scale). Each image is divided into I channels, the channels are equally spaced in terms of $\log(d_\mathrm{p})$, where $d_{\mathrm{p}i-1/2}$ and $d_{\mathrm{p}i+1/2}$ represent the lower and upper bounds of channel i. The response of each channel, R_i, is the number of particles counted in the channel.
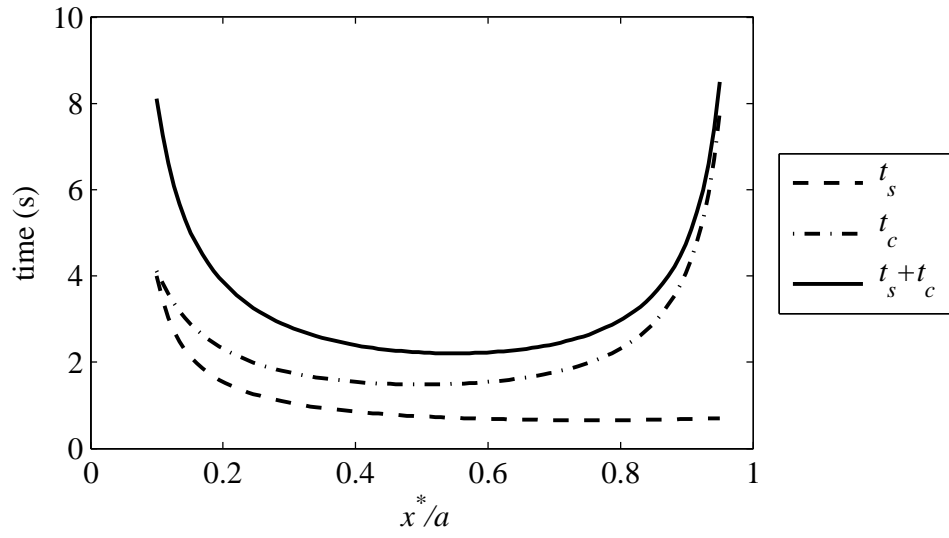
Fig. 3. The time each particle spends in the separator (t_s), the condenser (t_c), and the total ($t_\mathrm{s} + t_\mathrm{c}$) as a function of the particle location, $\tilde{x}^* = x^*/a$, for the operating conditions shown in Table 1.
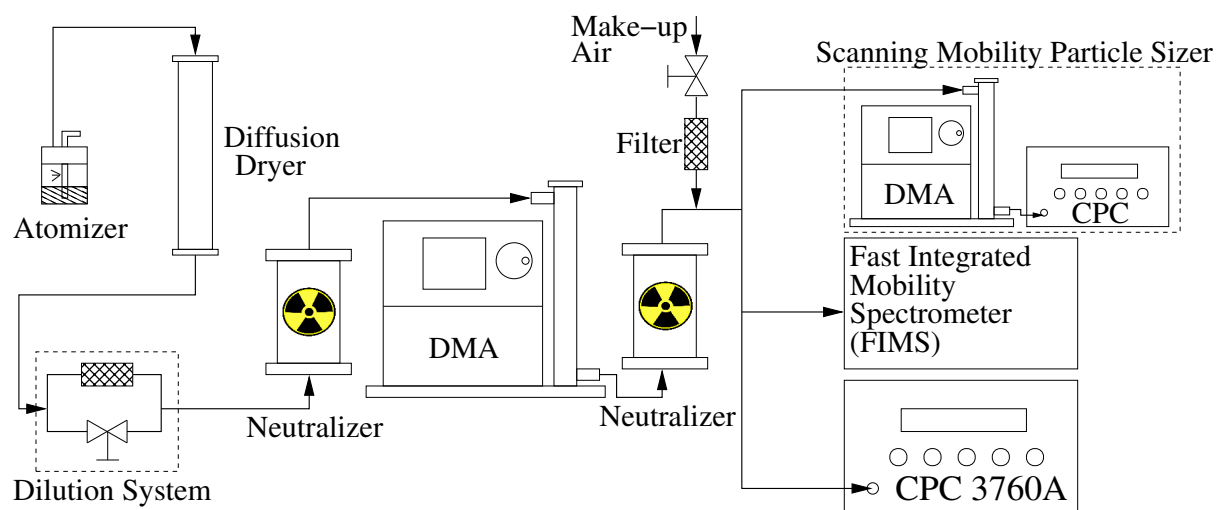
Fig. 4. Schematic of the experimental setup.
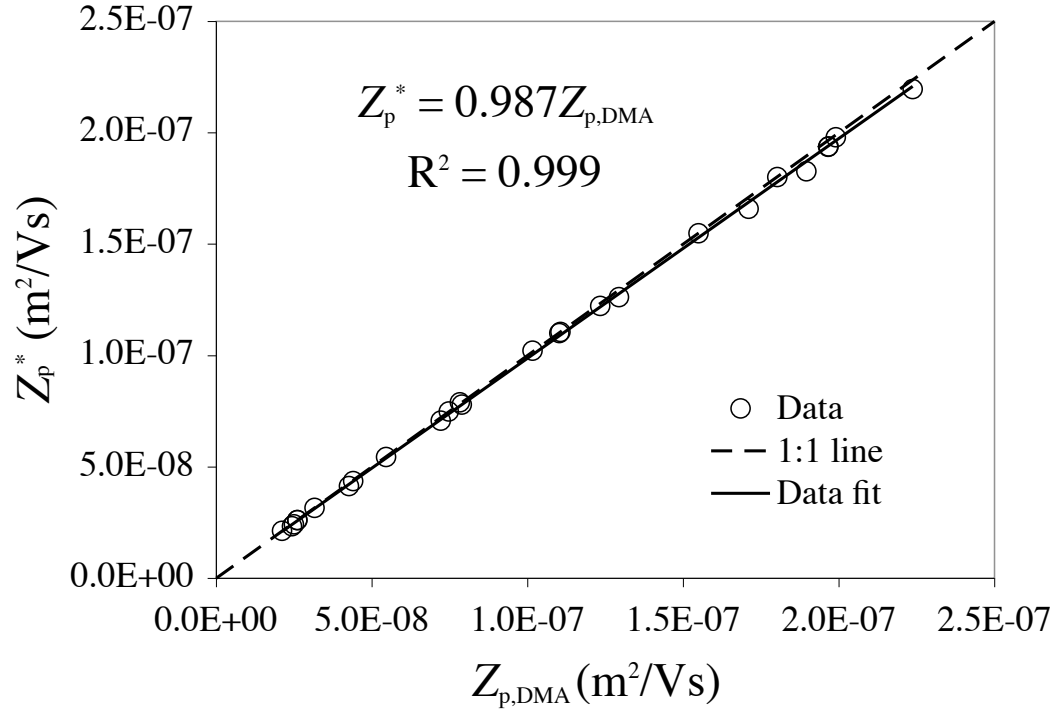
Fig. 5. Calibration curve for the FIMS, where $Z_{p,DMA}$ is the electrical mobility of particles from the DMA and Z_p^* is the expected instrument response electrical mobility of the FIMS (see Eq. 1).

(a)

(b)

(c)

(d)
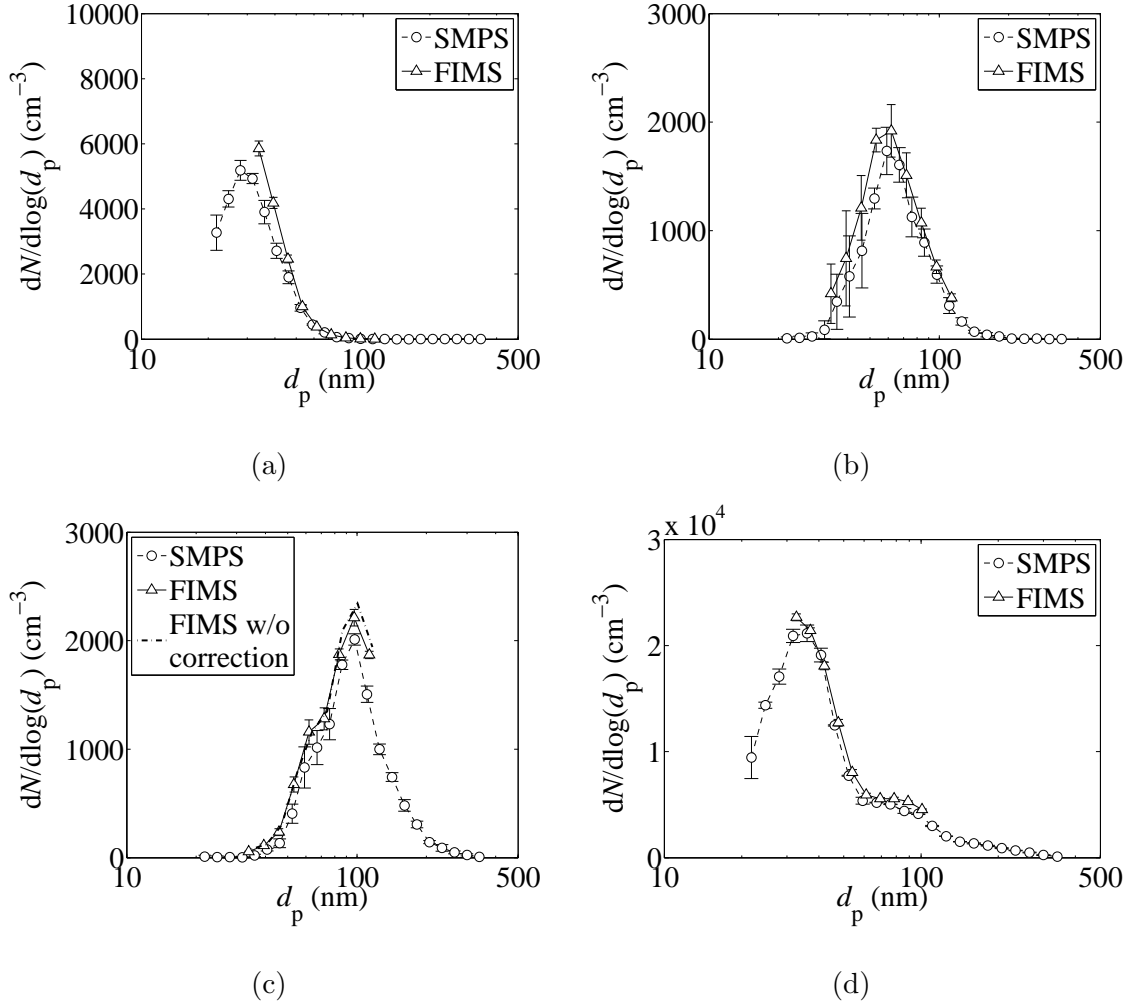
Fig. 6. Comparisons of aerosol size distributions measured with the FIMS and SMPS. Figures (a)–(c) are comparisons of DMA-classified NaCl particles. Figure (d) is a comparison of an ambient aerosol.
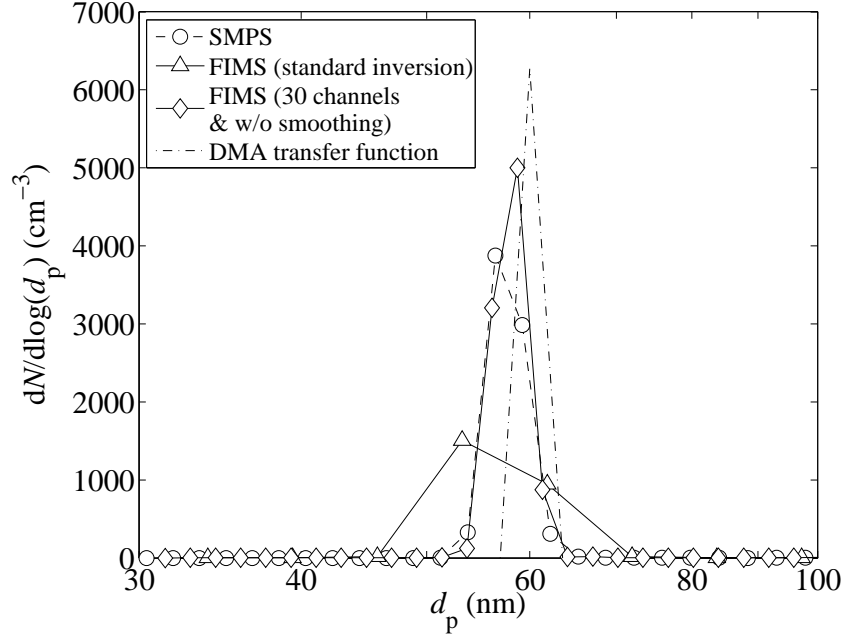
Fig. 7. Comparison of a 60 nm mono-disperse aerosol measured with the FIMS and SMPS. The FIMS inversion was carried out with the standard inversion (10 channels with smoothing, shown as '△') and with an inversion with 30 channels and without the smoothing function shown in Equation 12 (shown as '◇'). The expected distribution from the DMA (calculated from the operating conditions of the DMA) is also shown.
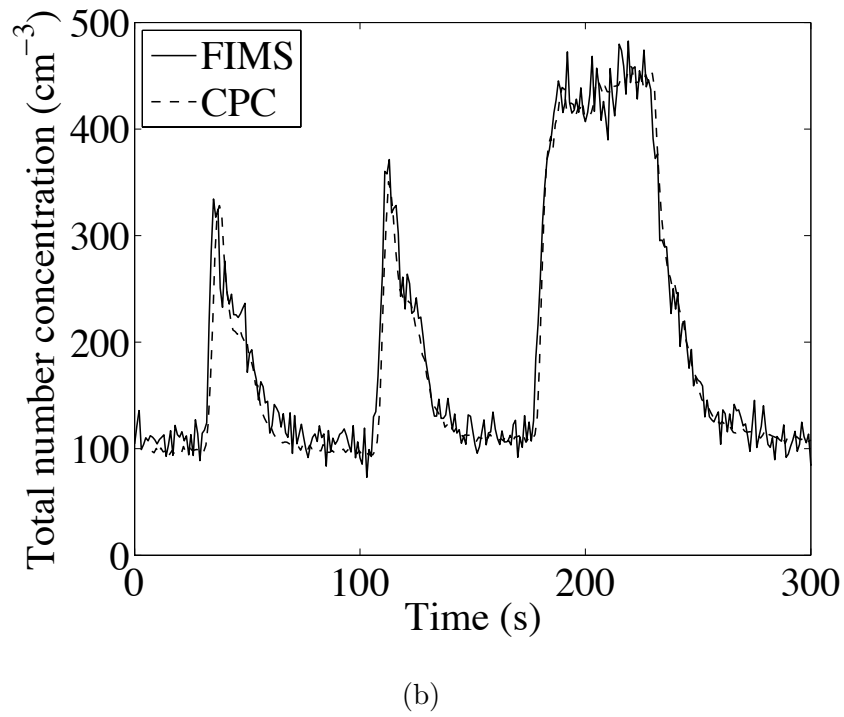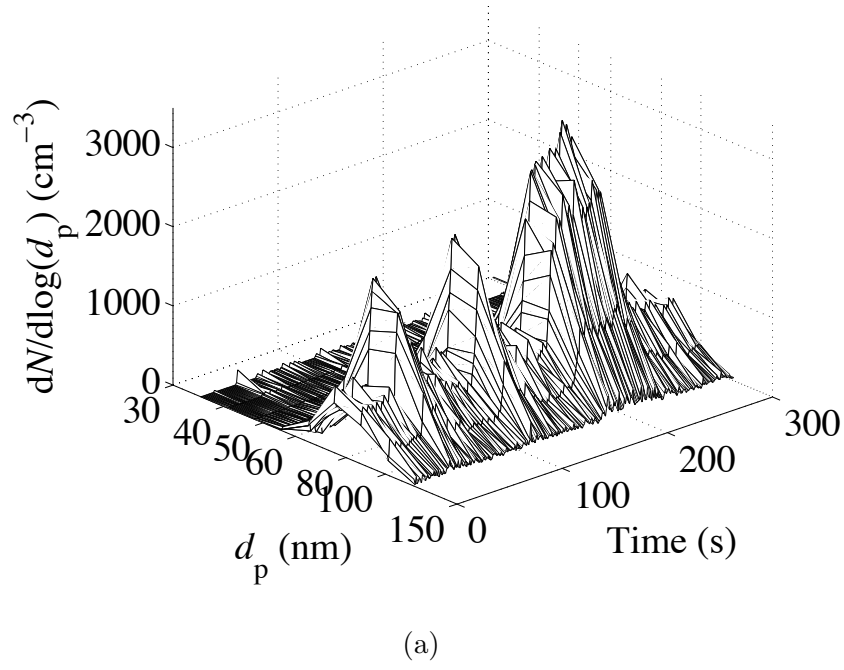
(a)

(b)

Fig. 8. Measurements of a transient aerosol: (a) size distribution measured with the FIMS, (b) total number concentration of the same aerosol measured with the FIMS and CPC.

40